Raman Investigation of Nanosized TiO2: Effect of Crystallite Size and Quantum Confinement

ARTICLE *in* THE JOURNAL OF PHYSICAL CHEMISTRY C · APRIL 2012

Impact Factor: 4.77 · DOI: 10.1021/jp2122196

9 AUTHORS, INCLUDING:

Wei Ji
Dalian University of Technology
30 PUBLICATIONS **363** CITATIONS
SEE PROFILE

Zhu Mao
Jilin University
16 PUBLICATIONS **169** CITATIONS
SEE PROFILE

Yue Wang
Jilin University
8 PUBLICATIONS **86** CITATIONS
SEE PROFILE

Weidong Ruan
Jilin University
52 PUBLICATIONS **878** CITATIONS
SEE PROFILE

THE JOURNAL OF PHYSICAL CHEMISTRY C

Article

pubs.acs.org/JPCC

Raman Investigation of Nanosized TiO_2: Effect of Crystallite Size and Quantum Confinement

Xiangxin Xue,[†] Wei Ji,[†] Zhu Mao,[†] Huijuan Mao,[†] Yue Wang,[†] Xu Wang,[†] Weidong Ruan,[†] Bing Zhao,*[,†] and John R. Lombardi[‡]

[†]State Key Laboratory of Supramolecular Structure and Materials, Jilin University, Changchun 130012, China

[‡]Department of Chemistry, The City College of New York, New York, New York 10031, United States

Supporting Information

ABSTRACT: The influence of the TiO_2 particle size on the enhanced Raman spectroscopy properties was systematically investigated on the nanometer-size scale. We report on the enhanced Raman spectrum of 4-mercaptobenzoic acid adsorbed on TiO_2 nanoparticles. The results presented in this study highlight the major findings that the intensities of both the molecular lines and the phonon modes of TiO_2 are strongly size-dependent. The TiO_2 crystallite size estimated using the Scherrer equation varied from 6.8 to 14.2 nm; as a function of crystal size, a large increase in intensity is observed, with a maximum near 10.9 nm and a subsequent decline at larger sizes. Moreover, we have investigated quantum confinement effects between TiO_2 and the adsorbed molecules and attribute this to a charge-transfer resonance, which is responsible for the Raman enhancement.

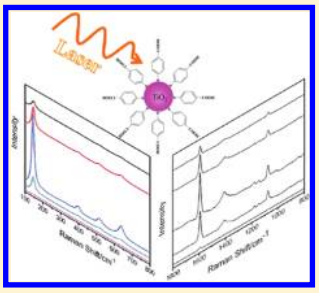

INTRODUCTION

Semiconductor nanocrystals are attractive candidates as active elements for nanoscale devices due to their different and enhanced physicochemical properties compared with their bulk counterparts.[1,2] In recent years, nanosized titanium dioxide (TiO_2) materials have elicited great interest because they exhibit many modified electronic and optical properties as well as extensive applications, including photocatalysis and photoelectrochemical solar cells.[3−5] Many methods, such as gas condensation,[6] sol−gel, and titanium-alkoxide hydrolysis, among others, have been successfully developed to prepare TiO_2 nanoparticles (NPs).[7]

However, it is still a major challenge to prepare semiconductor nanocrystals with controllable size, shape, and doping. Such NPs are of considerable interest since on the nanoscale, semiconductors exhibit unusual properties. If the diameter of a spherical particle (sometimes called a quantum dot) is smaller than the exciton Bohr radius, the valence and conduction bands divide into narrower bands due to quantum confinement effects on the electron and hole.[8] As the size is varied, the energy levels shift, with an increasing separation of valence and conduction bands with decreasing radius. This is sometimes referred to as a size-dependent increase in band gap. If a probe molecule is then adsorbed on the quantum dot surface, there is the possibility of light-induced charge-transfer between the adsorbate and the substrate, and the frequency of the charge-transfer resonance will vary with particle size. Such resonances can be scanned either by varying the excitation wavelength at fixed particle size or the particle size at fixed wavelength. The first observation of enhanced Raman spectroscopy on a semiconductor was reported by Quagliano on epitaxially grown InAs quantum dots.[9] We have observed such size dependent resonances in colloidal ZnO[10] quantum dots as well as in colloidal PbS quantum dots.[10,11]

With the development of nanosized materials, Raman spectroscopy has been popularly employed to investigate the nanostructures of titania. However, little research has been reported on the properties of surface enhanced Raman spectroscopy (SERS) of TiO_2. Rajh and co-workers have shown that the Raman signal of various biologically important molecules such as neurotransmitters can be enhanced by adsorption on a TiO_2 surface and that variations in the size of the particle can have a drastic effect on the Raman intensity.[12,13] Yang et al. reported that the SERS phenomenon may be attributed to a TiO_2-to-molecule charge-transfer mechanism.[7] Song et al. observed SERS signals when molecules are adsorbed on TiO_2−Ag NPs.[14] A more recent study showed enhancement of the TiO_2 phonon modes due to adsorption of several molecules.[15] In a more recent report using DFT calculations, the effects of quantum confinement, size, and solvent effects have been explored for formic acid and dopamine on TiO_2 NPs.[16] The authors showed that vibronic coupling is intimately tied to the strength of the Raman signal and that charge-transfer from the HOMO of the molecule to the conduction band of the quantum dot is the most likely mechanism. They also explored the strongly differing enhancements of various spectral normal modes.

To date, much effort has been dedicated toward enhanced Raman spectra of adsorbate, but seldom study has been focused on the phonon modes of semiconductor after molecules adsorbed on semiconductor NPs. Thus, in this article, we

Received: December 19, 2011
Revised: March 21, 2012
Published: March 27, 2012

   dx.doi.org/10.1021/jp2122196 | J. Phys. Chem. C 2012, 116, 8792−8797

report on recent results on the observation of the Raman results of 4-mercaptobenzoic acid (4-MBA) adsorbed on the surface of TiO_2 NPs. The size and monodispersity of the nanosized TiO_2 particles are carefully controlled, and we are able to construct a profile of the Raman signal as a function of particle size. Of particular interest was that the phonon modes of TiO_2 and the molecule lines were enhanced simultaneously.

EXPERIMENTAL SECTION

Chemical Reagents. 4-Mercaptobenzoic acid (4-MBA) was purchased from Acros Organics Chemical Co. and used as received without further purification. The other reagents (tetrabutyltitanate, anhydrous ethanol, and nitric acid) are all analytical grade. Triply distilled water was used for the entire synthesis.

Synthesis of TiO_2 NPs. Typically, TiO_2 NPs were synthesized by a sol-hydrothermal process using a previously reported procedure.[7] First, a mixed solution of 5 mL of tetrabutyltitanate and 5 mL of anhydrous ethanol were added dropwise into another mixed solution, consisting of 20 mL of anhydrous ethanol, 5 mL of water, and 1 mL of 70% nitric acid, which were roughly stirred to carry out hydrolysis at room temperature. Subsequently, the sol was obtained by continuously stirring for 1 h. Next, the as-prepared sol was sealed into a 50 mL Teflon-lined autoclave at 160 °C for 6 h, and then cooled to room temperature, followed by drying at 60 °C for 24 h. Finally, TiO_2 NPs were obtained by calcining the sol-hydrothermal production for 2 h at 400, 450, 500, 550, and 600 °C, respectively.

Adsorption of Probing Molecules. TiO_2 samples surface-modified by molecules were obtained as follows: first, 20 mg of TiO_2 NPs were dispersed in 10 mL of 4-MBA (1×10^{-3} M) and ethanol solution, and the mixture was stirred for 2 h. Second, the precipitate was centrifuged and rinsed with purified water three times. Finally, a small amount of powdered TiO_2 NPs modified by 4-MBA was placed on a glass slide for Raman measurement.

Sample Characterization. The crystal structure of TiO_2 NPs was characterized by X-ray diffraction using a Siemens D5005 X-ray powder diffractometer with a Cu Kα (λ = 1.5418 Å) radiation source at 40 kV and 30 mA. The surface morphology of the samples was measured on a Hitachi H-8100 transmission electron microscope (TEM) operated at an acceleration voltage of 200 kV. X-ray photoelectron spectra (XPS) were investigated by using a VG ESCALAB MK II spectrometer with an Mg KR excitation (1253.6 eV). The electronic absorption spectra were recorded on a Shimadzu UV-3600 UV−vis spectrophotometer. Raman spectra were measured with a Renishaw Raman system model 1000 spectrometer. The 514.5 nm line from a 20 mW air-cooled argon ion laser was used as the exciting light. Data acquisition was the result of three 10 s accumulations for molecules adsorbed on TiO_2 NPs. The resolution of the Raman instrument was ca. 4 cm^{-1}. The Raman band of the silicon wafer at 520.7 cm^{-1} was used to calibrate the spectrometer.

For Raman spectra, in order to properly compare the spectral intensities with particles of different size, we made a correction for the different surface area of the TiO_2 samples. Since the total mass of each sample was constant, assuming uniform coverage of each sample, the relative number of molecules interrogated by the laser in each sample is proportional to the area of a sphere. Thus, the intensity scales of the molecular Raman spectra below (Figures 6 and 7) were multiplied by a factor proportional to the surface area of the nanospheres.

RESULTS AND DISCUSSIONS

Structure and Composition of TiO_2 NPs. The properties of the TiO_2 NPs including crystal structure and composition will be demonstrated through a series of experiments. First, the crystalline structure of the TiO_2 NPs depends on the fabrication technique and the calcination temperature. XRD spectra were used to identify the size and structure of TiO_2 NPs. Figure 1 shows the XRD patterns of TiO_2 NPs calcined at

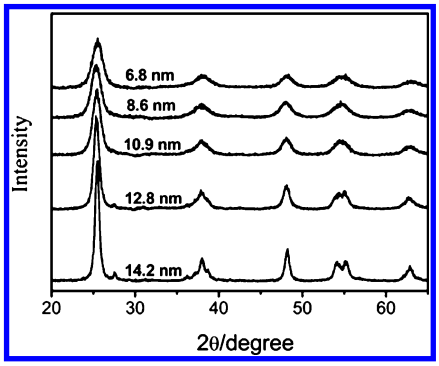

Figure 1. XRD spectra of TiO_2 nanoparticles with various sizes.

different temperatures. In general, the XRD peaks at 25.3° and 27.4° are identified as the characteristic diffraction peaks of the anatase and rutile crystal phase of TiO_2, respectively. Figure 1 reveals that TiO_2 NPs calcined from 400 to 500 °C were pure anatase phase TiO_2. Increasing the calcination temperature up to 550 °C showed the appearance of a small amount of rutile phase. We have observed that the diffraction peaks increase in intensity and narrow in width with the calcination temperature rising from 400 to 600 °C, indicating that the degree of crystallinity of samples and the crystalline size increases. The crystallite sizes (D) were about 6.8, 8.6, 10.9, 12.8, and 14.2 nm, respectively. These values were estimated from the half-bandwidth of the corresponding X-ray spectral peak by the Scherrer formula: $D = k\lambda/(\beta \cos \theta)$, where λ is the X-ray wavelength, β is the half width of the (110) peak, θ is the Bragg diffraction angle, and k is a correction factor, which is taken as 0.89.[17] The TEM results also confirm this (see Supporting Information Figure S1).

To further examine the character of TiO_2 NPs, the state of Ti in TiO_2 NPs measured by XPS was obtained. The Ti_{2p} and O_{1s} XPS spectra of the TiO_2 NPs are shown in Figure 2. Binding energy positions of Ti $2p_{3/2}$ and Ti $2p_{1/2}$ for the TiO_2 were estimated to be 458.3 and 464.0 eV, respectively. The observed peak positions, the doublet separation between the $2p_{1/2}$ and $2p_{3/2}$ peaks of ~5.7 eV, are characteristic of TiO_2.[18]

Spectroscopy Studies of TiO_2 NPs. To investigate the interaction between TiO_2 and the adsorbed molecules, the UV−vis spectra were obtained (Figure 3). Under ultraviolet irradiation, electrons in the valence band absorb the photon energy and jump to the conduction band, leaving holes in the valence band. The intense absorption edge observed in the range below 410 nm is associated with the band−band transition of the TiO_2 NPs according to its intrinsic bandgap. Another principal feature is that the absorption edge of 4-MBA modified TiO_2 shifts to longer wavelengths compared with that of TiO_2. This shift can be interpreted as the result of the

dx.doi.org/10.1021/jp2122196 | J. Phys. Chem. C 2012, 116, 8792−8797

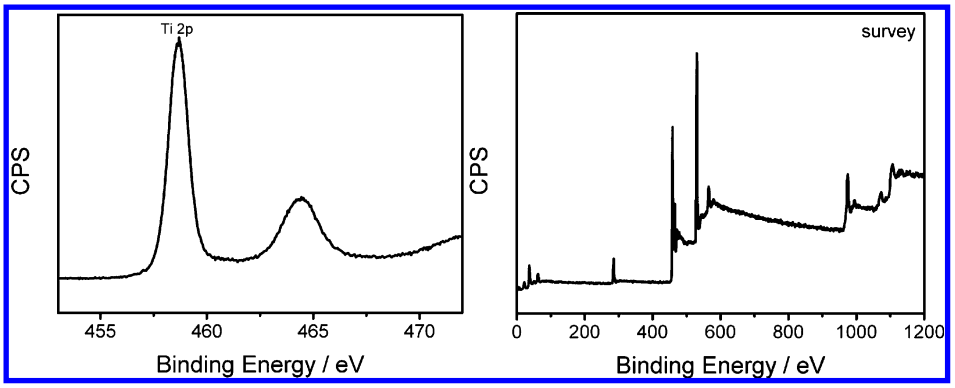

Figure 2. XPS spectra of TiO_2 nanoparticles.

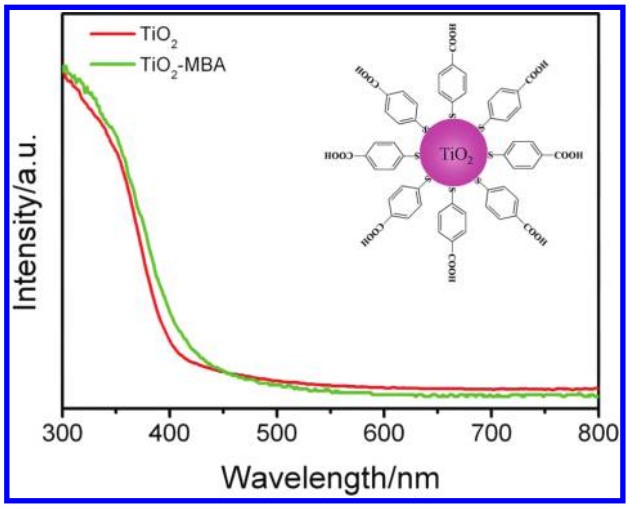

Figure 3. UV−vis DRS spectra of TiO_2 and 4-MBA adsorbed on the 8.6 nm diameter TiO_2 NPs; inset, the sketch of 4-MBA adsorbed on TiO_2 nanoparticles.

appreciable influence of molecules adsorbed on TiO_2 NPs. The likely orientation of the 4-MBA modified TiO_2 NPs is shown in the inset of Figure 3. Similar results have been obtained for dye molecules adsorbed on TiO_2 surfaces and for 4-MPY surface-modified CuO NPs.[19,20]

To determine the bandgap of nanocrystalline TiO_2 with different diameters, absorption spectra of the powder (Figure 4) were obtained for the wavelengths in the range of 300−800 nm. The bandgap (E_g) was calculated using the equation;

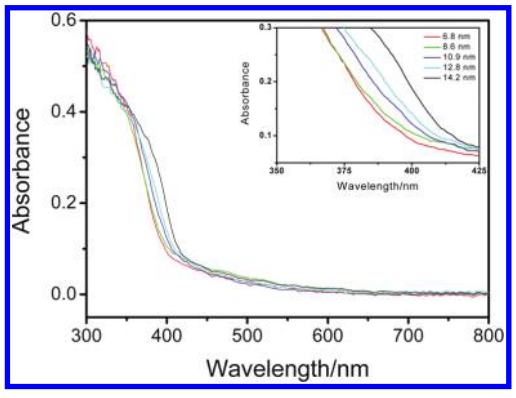

Figure 4. UV−vis DRS spectra of TiO_2 nanoparticles with various sizes.

bandgap as a function of particle size (d) can be fit to a function of the form[21]

$$E_g = 3.2 + \frac{0.0186}{1 - 0.236d + 0.019d^2} \quad (1)$$

where the bulk band gap is 3.2 eV. With increasing TiO_2 diameter, the absorbance in the range below 410 nm is noted to increase. As shown in the inset, a systematic red shift in the absorbance spectra with increasing diameter is clearly seen. It is well-known that, when the radius of a spherically shaped semiconductor particle is reduced to that of the semiconductor Bohr radius or less, the bandgap increases and becomes size dependent due to quantum confinement effects. In this work, the shift in the absorbance is distinctly noticeable with the calculated bandgap of 3.268, 3.25, 3.227, 3.217, and 3.213 eV, respectively.

The Raman spectra collected from the pyrogenic TiO_2 NPs in the region of 100−800 cm^{-1} are shown in Figure 5, and for ease of comparison, they are also shown normalized to the intensity of the $E_g(1)$ peak (147 cm^{-1}). The wavenumbers and the full widths at half-maximum (fwhm) of this band are given in Table 1 (by Gaussian fit). By comparing the Raman spectra, it is clear that the Raman bands shift toward lower wavenumber and that their intensities increase relatively as the particle size increases. The TiO_2 crystallinity increases with increasing the calcination temperature, while simultaneously the surface area and surface defect content of TiO_2 nanoparticles also decreases. This results in changes to the fwhm. These results are comparable to those previously obtained in anatase nanocrystals of TiO_2 by Bersani and Lottici,[22] as well as Swamy et al.[23] When the particle size becomes sufficiently small, the usual rule of conservation of momentum, which leads to the selection rule that $q \approx 0$ (q is the momentum vector), breaks down and is replaced by the q-vector relaxation model. In this, the phonon dispersion is invoked resulting in expressions of the following type:[23]

$$\Delta\omega = k_1(1/L^{\alpha}) \quad (2)$$

$$\Gamma = k_2(1/L^{\alpha}) + \Gamma_0 \quad (3)$$

where $\Delta\omega$ is the shift in frequency, and Γ is the line width. α is a scaling parameter that is related to the network structure, and L is the particle size. In Figure 6, we display fits of our data to these expressions. From the observed profiles in Figure 6, α is found to be 1.497; the standard deviation of the fit was found to be 9.8. The other parameters were k_1 =128.7, k_2 = 226.1, and Γ_0 = 8.99. Previous reports indicate that, for covalently bonded

dx.doi.org/10.1021/jp2122196 | J. Phys. Chem. C 2012, 116, 8792−8797

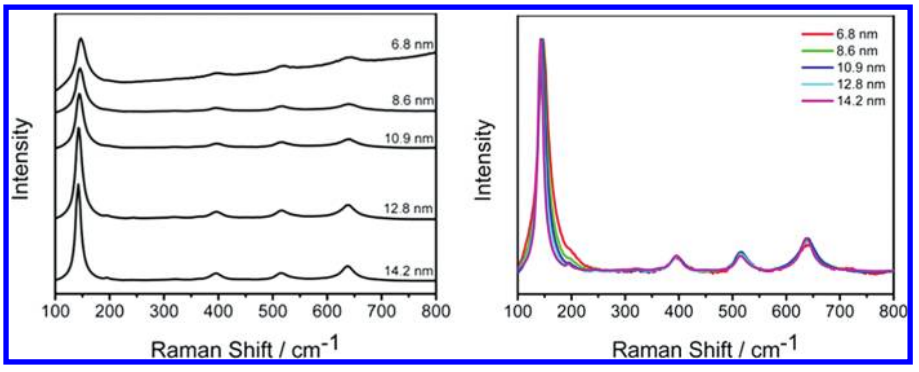

Figure 5. Raman spectra of TiO_2 nanoparticles (bare) at various sizes (left) and the normalized picture (right).

Table 1. Gaussian Fit of the Wavenumber and the fwhm of the $E_g(1)$ Phonon Mode of the Five Samples (cm^{-1})

TiO_2 diameter (nm)	wavenumber (nm)	fwhm (nm)
6.8	147.3	21.9
8.6	146.5	18.3
10.9	145.1	16.4
12.8	143.7	14.1
14.2	142.6	12.2

semiconductors such as Si and GaAs, α is ~1.5. Our fits are entirely consistent with these results.

In the experiment, besides the Raman spectra of the bare TiO_2 NPs, a study of the adsorbents has also been carried out. Figure 7 shows the Raman spectra of 4-MBA on TiO_2 NPs of various sizes in the range between 6.8 and 14.2 nm diameters. Note that the maximum signal is observed when the TiO_2 diameter is 10.9 nm. The SERS signal will increase with decreasing particle size until the size quantization regime is reached at which point SERS enhancement is expected to diminish due to the decrease in the vibronic coupling between allowed discrete states. The strong Raman bands at about 1594 and 1087 cm^{-1} can be attributed to ν_{8a} (a_1) and ν_{12} (a_1) aromatic ring characteristic vibrations, respectively. Other weak bands such as 1145 (ν_{15}, b_2) and 1183 (ν_9, a_1) cm^{-1} correspond to the C−H deformation modes and agree well with the literature data.[10] In Table 2, we list the observed SERS spectrum of 4-MBA on Ag (Au) NPs. The enhancement factor of pure TiO_2 has been calculated for about 3.5×10^3.[24]

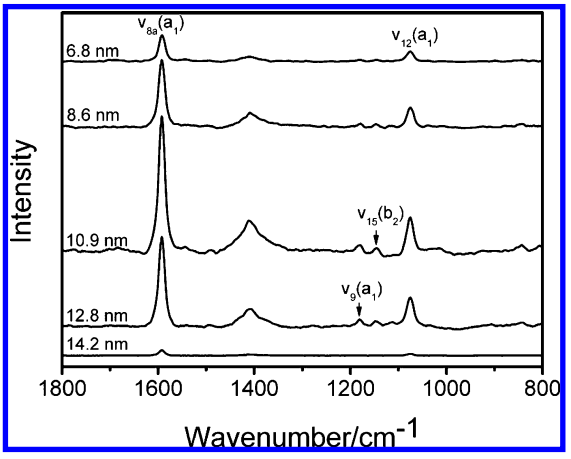

Figure 7. Raman spectra of 4-MBA adsorbed on TiO_2 nanoparticles with various sizes. Relative intensities were corrected for varying surface area of the samples.

Another interesting point is that we also observed enhanced Raman intensity of the phonon modes of TiO_2 NPs induced by adsorption of 4-MBA (Figure 8) compared to the unmodified TiO_2 NPs (Figure 2). Because the concentration of 4-MBA is in excess, it is likely that the adsorbate forms a monolayer on the surface. Note the maximum signal again is observed when the TiO_2 diameter is 10.9 nm.

In order to observe the size dependent tendency more clearly, we plot the intensity of the 1594 cm^{-1} band of 4-MBA as a function of particle size. As the particle diameter is increased, the Raman intensity increases, until a maximum is

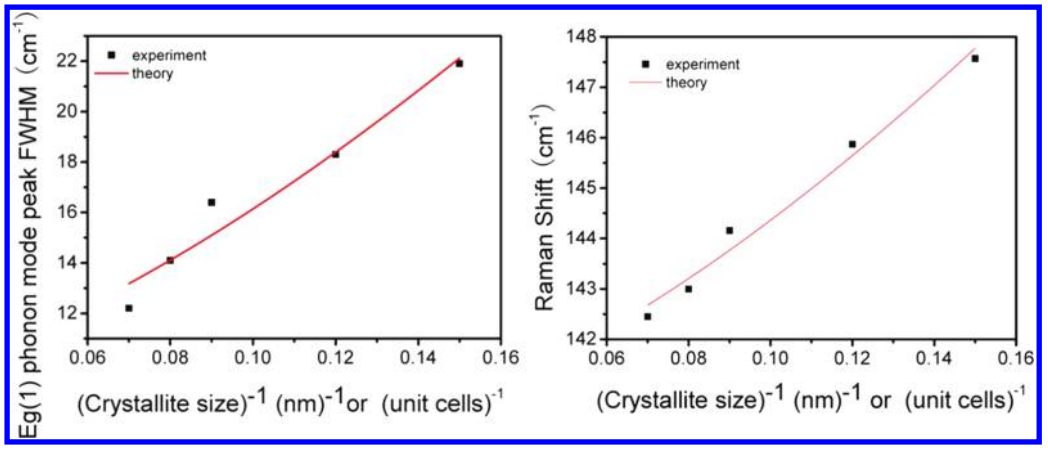

Figure 6. Correlations of the crystallite size and the peak positions of the $E_g(1)$ phonon mode peak (left) and the Raman line widths (right).

dx.doi.org/10.1021/jp2122196 | J. Phys. Chem. C 2012, 116, 8792−8797

Table 2. Raman Shifts and Assignments of 4-MBA Molecule[a]

Raman	SERS		
bulk	on Ag (Au)	on TiO_2	assignment
			νCO
1623 w			νCO
1596 s	1590(1588) s	1594 s	νCC, (a_1)
1182 m	1186 w	1182 w	νCH, 9 (a_1)
		1148 vw	νCH, 15 (b_2)
1098 s	1080(1077) m	1078 m	νCC, 12 (a_1)
913 vw			δCSH, 9b (b_2)
806 w			δOCO

[a]Assignments are from ref 25; s = strong, m = medium, w = weak, vw = very weak.

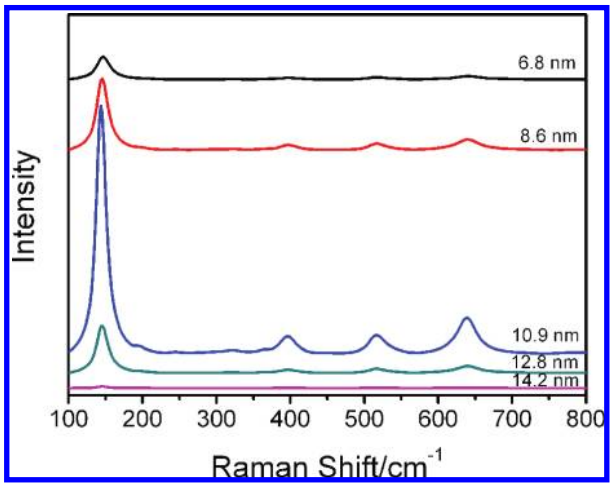

Figure 8. Raman spectra of TiO_2 nanoparticles after modification with 4-MBA.

reached at 10.9 nm, then decreases (Figure 9, black line). We can then take the ratio of intensities of the lines with molecules adsorbed to that of the bare TiO_2 spectrum as the enhancement factor (EF). We also plot the EF value as a function of different TiO_2 diameters (Figure 9, blue dotted line). We obtain a maximum at the same diameter.

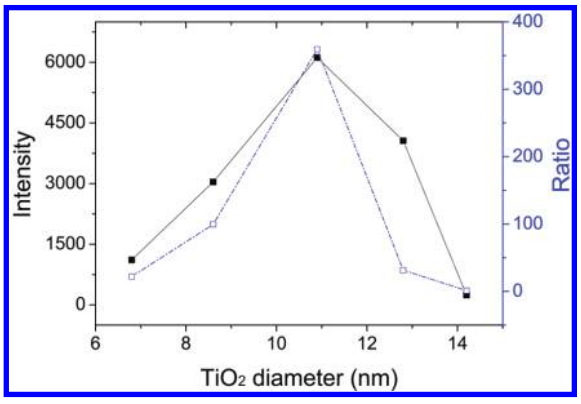

Figure 9. Raman intensity of the 1594 cm^{-1} mode of 4-MBA adsorbed on TiO_2 nanoparticles (black line). The data show an average of 5 independent measurements at different locations on the sample. The enhancement factor (EF) value as a function of TiO_2 diameter (blue dotted line).

It is generally accepted that there are two types of mechanisms that can contribute to the SERS enhancement: the first is the electromagnetic enhancement, which is caused by a strong surface plasmon resonance of the nanoparticle metal surface coupled to the incident light.[26,27] The second is the chemical enhancement, which can be considered similar to a resonance Raman process between the ground electronic state of the molecule−metal complex and its new excited levels arising from charge transfer between the metallic surface and the adsorbed molecule.[28−30] It should be noted that, for most semiconductor materials, the dominant contribution for the SERS signal must be a charge-transfer mechanism since surface plasmon resonances lie far in the infrared. In this TiO_2 system, the SERS signals have been attributed to the TiO_2-to-molecule charge-transfer mechanism. That is, the electrons are excited from the valence band of TiO_2 to the energy of the surface states and then injected into the LUMO orbital of the adsorbed molecules. The bandgap energy of TiO_2 nanoparticles has been shown to vary with particle diameter. Using their experimental data, bandgap as a function of particle size can be fit to a function (eq 1).[21] This function is strongly varying in the vicinity of d = 10−11 nm. However, there is still insufficient experimental data to determine the exact variation of the separate valence or conduction bands in this vicinity. However, the onset of large deviation from the bulk bandgap in the region of our experiments indicates that a size-dependent charge-transfer resonance is the most likely explanation of our results.

However, Rajh and co-workers have come to the opposite conclusion for formic acid and dopamine, i.e., that the direction of charge-transfer is from the HOMO of the molecule to the conduction band of the semiconductor.[12] The direction of charge-transfer is dependent on the energy of the HOMO and LUMO of the molecule with respect to the conduction and valence bands of the semiconductor quantum dot. It is even conceivable that the direction could change with size. However, for 4-MBA acid, the ionization potential is 8.48 eV, while the conduction band of TiO_2 lays 4.2 eV below the vacuum level.[31] This makes it impossible for transitions from the molecule to the semiconductor conduction band to take place in the visible region of the spectrum, while transitions from the valence band of TiO_2 to the LUMO of the molecule are well within the spectral range of these experiments.

Because of quantum confinement, the energy of the valence band varies strongly with particle size, and at fixed excitation wavelength, we expect a resonance to be obtained when the particle size resonance corresponding to the excitation energy is attained. This result is very similar to our recent report of a size-dependent resonance in 4-mercaptopyridine adsorbed on PbS quantum dots.[11] The resonance was found to be at about 8 nm. In that case, there existed sufficient experimental data to plot the conduction band and valence band as a function of particle size and identify clearly the transition from which the charge-transfer resonance arises. The location of the gap between the valence band of the quantum dots and the molecular LUMO almost exactly matched the excitation energy of the laser. We expect that, when sufficient information is available concerning the exact location of the valence band of TiO_2, we will be able to obtain a corresponding confirmation of our assignment.

CONCLUSIONS

In summary, TiO_2 NPs with various sizes were fabricated by a sol-hydrothermal method for Raman studies. Nanoparticle size is an important parameter affecting the Raman intensity. In this

dx.doi.org/10.1021/jp2122196 | J. Phys. Chem. C 2012, 116, 8792−8797

work, results are obtained that both the surface enhanced Raman spectra and the phonon modes of TiO_2 are enhanced when 4-MBA adsorbed on TiO_2 NPs as a function of nanoparticle size. By making use of size quantization effects, one can readily tune the Raman intensity, which enhancement attains a maximum value at particle size 10.9 nm at the exciting wavelength (514.5 nm). This is most likely due to a charge-transfer resonance between the valence band of TiO_2 and the lowest unoccupied orbital of the molecule. Note that the variation of Raman signal with particle size enables us to determine the configuration of the nanoparticle, which optimizes the intensity. This has important implications for the design of sensors based on semiconductor quantum dots, as well as for the construction of solar cells. In order to construct the most highly sensitive molecular sensors, we must know which particle configuration gives the largest Raman signal. For solar cells to be of the highest efficiency, we must know how to produce the highest rate of charge-transfer. At least for TiO_2 quantum dots, we have shown that an optimum signal and maximum charge-transfer is obtained at 10.9 nm for 4-mercaptobenzoic acid. The exact optimum size will clearly depend on the nature of the molecular adsorbate, but we have shown here how to best determine the optimum parameters needed.

■ ASSOCIATED CONTENT

Supporting Information

TEM results. This material is available free of charge via the Internet at http://pubs.acs.org.

■ AUTHOR INFORMATION

Notes

The opinions, findings, and conclusions or recommendations expressed in this publication/program/exhibition are those of the author(s) and do not necessarily reflect those of the Department of Justice.

The authors declare no competing financial interest.

■ ACKNOWLEDGMENTS

This study was supported by the National Natural Science Foundation (Grant Nos. 20873050, 20921003, and 20973074) of P. R. China; the 111 project (B06009). We are indebted to the support of the National Science Foundation (NSF-SCIART) Grant No. CHE-1041832. This project was also supported by Award No. 2006-DN-BX-K034 awarded by the National Institute of Justice, Office of Justice Programs, U.S. Department of Justice.

■ REFERENCES

(1) Zayats, M.; Kharitonov, A. B.; Pogorelova, S. P.; Lioubashevski, O.; Katz, E.; Willner, I. *J. Am. Chem. Soc.* **2003**, *125*, 16006.
(2) Guo, Y. G.; Hu, J. S.; Liang, H. P.; Wan, L. J.; Bai, C. L. *Adv. Funct. Mater.* **2005**, *15*, 196.
(3) Carp, O.; Huisman, C. L.; Reller, A. *Prog. Solid State Chem.* **2004**, *32*, 33.
(4) Gratzel, M. *Nature* **2001**, *414*, 338.
(5) Gao, E. Q.; Li, Z.; Yang, M. Z.; Cai, S. M. *Acta Phys.-Chim. Sin.* **2001**, *17*, 177.
(6) Levchenko, A. A.; Li, G. S.; Boerio-Goates, J.; Woodfield, B. F.; Navrotsky, A. *Chem. Mater.* **2006**, *18*, 6324.
(7) Yang, L. B.; Jiang, X.; Ruan, W. D.; Zhao, B.; Xu, W. Q.; Lombardi, J. R. *J. Phys. Chem. C* **2008**, *112*, 20095.
(8) Voskoboynikov, O.; Lee, C. P.; Tretyak, O. *Physical Review B* **2001**, *63*, 165306.
(9) Quagliano, L. G. *J. Am. Chem. Soc.* **2004**, *126*, 7393.
(10) Sun, Z. H.; Zhao, B.; Lombardi, J. R. *Appl. Phys. Lett.* **2007**, *91*, 221106.
(11) Fu, X.; Pan, Y.; Wang, X.; Lombardi, J. R. *J. Chem. Phys.* **2011**, *134*, 024707.
(12) Musumeci, A.; Gosztola, D.; Schiller, T.; Dimitrijevic, N. M.; Mujica, V.; Martin, D.; Rajh, T. *J. Am. Chem. Soc.* **2009**, *131*, 6040.
(13) Tarakeshwar, P.; Finkelstein-Shapiro, D.; Hurst, S. J.; Rajh, T.; Mujica, V. *J. Phys. Chem. C* **2011**, *115*, 8994.
(14) Song, W.; Wang, Y. X.; Zhao, B. *J. Phys. Chem. C* **2007**, *111*, 12786.
(15) Ma, S.; Livingstone, R.; Zhao, B.; Lombardi, J. R. *J. Phys. Chem. Lett.* **2011**, *2*, 671.
(16) Tarakeshwar, P.; Finkelstein-Shapiro, D.; Rajh, T.; Mujica, V. *Int. J. Quantum Chem.* **2011**, *111*, 1659.
(17) Swamy, V.; Muddle, B. C.; Dai, Q. *Appl. Phys. Lett.* **2006**, *89*, 163118.
(18) Stefanov, P.; Shipochka, M.; Stefchev, P.; Raicheva, Z.; Lazarova, V.; Spassov, L. *Proceedings of the 17th International Vacuum Congress/13th International Conference on Surface Science/International Conference on Nanoscience and Technology*, 2008; Vol. *100*.
(19) Leon, C. P.; Kador, L.; Peng, B.; Thelakkat, M. *J. Phys. Chem. B* **2006**, *110*, 8723.
(20) Shoute, L. C. T.; Loppnow, G. R. *J. Am. Chem. Soc.* **2003**, *125*, 15636.
(21) Lee, S.; Cho, I.-S.; Noh, J.-H.; Hong, K. S.; Han, G. S.; Jung, H. S.; Jeong, S.; Lee, C.; Shin, H. *Phys. Status Solidi A* **2010**, *207*, 2288.
(22) Bersani, D.; Lottici, P. P.; Ding, X. Z. *Appl. Phys. Lett.* **1998**, *72*, 1.
(23) Swamy, V.; Kuznetsov, A.; Dubrovinsky, L. S.; Caruso, R. A.; Shchukin, D. G.; Muddle, B. C. *Phys. Rev. B* **2005**, *71*, 184302.
(24) Wang, Y.; Ruan, W.; Zhang, J.; Yang, B.; Xu, W.; Zhao, B.; Lombardi, J. R. *J. Raman Spectrosc.* **2009**, *40*, 1072.
(25) Michota, A.; Bukowska, J. *J. Raman Spectrosc.* **2003**, *34*, 21.
(26) Lombardi, J. R.; Birke, R. L. *Acc. Chem. Res.* **2009**, *42*, 734.
(27) Schatz, G. C.; Young, M. A.; Van Duyne, R. P. In *Surface-Enhanced Raman Scattering: Physics and Applications*; Kneipp, K., Moskovits, M., Kneipp, H., Eds.; Springer: New York, 2006; Vol. *103*, p 19.
(28) Moskovits, M. *J. Raman Spectrosc.* **2005**, *36*, 485.
(29) Otto, A. *J. Raman Spectrosc.* **2005**, *36*, 497.
(30) Otto, A.; Futamata, M. In *Surface-Enhanced Raman Scattering: Physics and Applications*; Kneipp, K., Moskovits, M., Kneipp, H., Eds.; Springer: New York, 2006; Vol. *103*, p 147.
(31) Cook, M. J.; El-Abbady, S.; Katritzky, A. R.; Guimon, C.; Pfister-Guillouzo, G. *J. Chem. Soc., Faraday Trans. II* **1977**, *68*, 1652.